Journal of Catalysis **204,** 53–63 (2001)
doi:10.1006/jcat.2001.3375, available online at http://www.idealibrary.com on IDEAL®

Effects of Single-File Diffusion on the Kinetics of Hydroisomerization Catalyzed by Pt/H–Mordenite

F. J. M. M. de Gauw,[1] J. van Grondelle, and R. A. van Santen

Schuit Institute of Catalysis, Eindhoven University of Technology, P.O. Box 513, 5600 MB Eindhoven, The Netherlands

Received February 12, 2001; revised May 16, 2001; accepted July 31, 2001

The hydroisomerization of *n*-hexane on large crystals (50 μm) of Pt-loaded H–mordenite has been used as a test reaction to study the effects of concentration-dependent diffusion on zeolite catalyzed reactions. This concentration dependence was observed in the form of a nonlinear deviation from the relation between the reaction rate and the *n*-hexane pressure as provided by the intrinsic reaction rate equation. The dependence of the activity on the *n*-hexane pressure was measured at various temperatures and the results were compared with the results of model calculations. In the model used for these simulations it was assumed that the effective diffusion coefficient was proportional to $(1-\theta)/\theta$ (θ = fraction of occupied sites) as proposed by K. Hahn and J. Kärger (*J. Phys. Chem. B* 102, 5766 (1998)) and P. H. Nelson and S. M. Auerbach (*J. Chem. Phys.* 110, 9235 (1999)) for single-file diffusion at long times. Furthermore, since it is thought that immobile alkoxy intermediates are present in the pores under reaction conditions, it was assumed that the effective diffusion coefficient was proportional to the fraction of surface species consisting of hexanes and hexenes. Except for the effective single-particle diffusion coefficient, for which no reliable literature value was found, independently obtained input parameters were used in the model calculations. Good agreement between experiment and model was obtained using a value for the effective single-particle diffusion coefficient of $\sim 10^{-5}$ m^2/s, which is well within the range of orders observed for the single-particle diffusion coefficients of methane and tetrafluormethane in molecular sieves.

Key Words: **zeolites; hydroisomerization; single-file diffusion; alkoxy species; kinetic modeling.**

INTRODUCTION

Nowadays, numerous industrial processes involve the use of zeolitic and related microporous catalysts. Since the dimensions of cages and pores in these materials are usually comparable to those of reactant and product molecules, there is in many cases too little space for counterdiffusion of adsorbed molecules. Because in this situation molecules can only move to a site if it is unoccupied, the motion of individual molecules is correlated (at least for short observation times) and the mobility will decrease with increasing occupancy and decreasing connectivity of the pore system.

Here we present results of a study on the effects of diffusion on the kinetics of *n*-hexane hydroisomerization catalyzed by Pt/H–mordenite. As the cross section of the pores (6.5×7.0 Å) is smaller than twice the kinetic diameter of *n*-hexane (4.3 Å (1)) and the micropores are one-dimensional, adsorbed molecules cannot exchange their positions and can only move to a given point in the pore if all intermediate molecules are displaced beyond this point. This type of molecular transport is called single-file diffusion. Since effects of diffusion on reaction kinetics will only emerge if the average residence time of molecules in the micropores is at least of the same order of magnitude as the typical lifetime of an adsorbed reactant molecule, a catalyst consisting of relatively large crystals (50 μm) was used. The hydroisomerization of *n*-hexane on Pt/H–mordenite is a particularly interesting system for various reasons. In the first place, the hydroisomerization of mixtures of *n*-hexane and *n*-pentane belongs to the most widely operated oil-refining processes and Pt/H–mordenite is one of the two catalysts that is commercially used, the other being Pt on chlorinated alumina (2). The purpose of hydroisomerization is to convert *n*-pentane and *n*-hexane into branched alkanes, which are more suitable for use as motor fuel because of their higher octane number. In the second place, the presence of strongly bonded reaction intermediates (alkoxy species) which have been predicted by quantum chemical calculations (3, 4) may have anomalous effects on the hydroisomerization kinetics in addition to the effects caused by single-file diffusion.

In order to assess the effect of single-file diffusion on the reaction kinetics, a rate equation representing the intrinsic kinetics is required. Such an equation can be derived assuming that the bifunctional mechanism for hydroisomerization as proposed by Weisz (5) is valid. According to this mechanism, an isomer is obtained by (i) dehydrogenation of the adsorbed alkane, (ii) protonation of the resulting alkene, giving a stable alkoxide intermediate, and

[1] To whom correspondence should be addressed. E-mail: F.J.M.M.de.Gauw@tue.nl. Fax: (31) 40 245 5054.

0021-9517/01 $35.00

(iii) isomerization of the alkoxide, followed by the reverse of steps (ii) and (i) (deprotonation and hydrogenation). The mechanism is called bifunctional because two catalytic functions are involved, a Pt function for (de)hydrogenation and an acid function for (de)protonation and isomerization. If it is assumed that adsorption can be described by a Langmuir isotherm, that the isomerization step is rate determining, and that the reverse reaction can be neglected, the equation obtained (see Appendix) is

$$TOF = k_{isom}\theta_{nC6\,alkoxy} = \frac{k_{isom}K_{ads}K_{dehydr}K_{prot}\frac{p_{nC6}}{p_{H_2}}}{1 + K_{ads}p_{nC6} + K_{ads}K_{dehydr}\frac{p_{nC6}}{p_{H_2}} + K_{ads}K_{dehydr}K_{prot}\frac{p_{nC6}}{p_{H_2}}}, \quad [1]$$

where k_{isom} is the rate coefficient of isomerization of the *n*-hexyl alkoxide; and $\theta_{nC6\,alkoxy}$ is the surface occupancy of the *n*-hexyl alkoxide; K_{ads}, K_{dehydr}, and K_{prot} are the equilibrium constants, respectively, of adsorption, dehydrogenation, and protonation of *n*-hexane; and p_{nC6} is the partial pressure of *n*-hexane and p_{H_2} of hydrogen. Equations similar to Eq. [1] have been proposed by Ribeiro *et al.* (6) and Froment (7). However, in deriving these equations it has been assumed that the surface concentration of alkanes and alkenes can be neglected, which a priori is not necessarily a good approximation. Equation 1 can be rewritten in a linear form by taking the reciprocal:

$$\frac{1}{TOF} = \frac{1}{k_{isom}} + \frac{1}{k_{isom}K_{prot}} + \frac{p_{H_2}}{k_{isom}K_{dehydr}K_{prot}} + \frac{p_{H_2}}{k_{isom}K_{ads}K_{dehydr}K_{prot}}\frac{1}{p_{nC6}}. \quad [2]$$

According to Eq. [2], plots of $1/TOF$ versus $1/p_{nC6}$, which we will refer to as reciprocal rate equation plots, should be linear. However, if diffusion limitation occurs and the diffusion coefficient decreases with increasing concentration, as in single-file diffusion (see below), reciprocal rate equation plots can be expected to be nonlinear, because with varying $1/p_{nC6}$ the resulting linear variation of the intrinsic $1/TOF$ is counteracted by a nonlinear variation of the rate of mass transfer. It should be mentioned that for a reaction that is first order in θ, such as the hydroisomerization reaction, diffusion limitation will not lead to nonlinear deviations from the reaction rate equation if the diffusion coefficient is concentration-independent. This is a result of the fact that in this case the effectiveness factor (the ratio between the reaction rate under conditions of diffusion limitation and the intrinsic reaction rate) is independent of θ (8), so that irrespective of the reactant pressure the reaction rate is reduced by the same factor.

The kinetic experiments comprise of measuring the *TOF* of the large crystals of Pt/H–mordenite as a function of n-hekane pressure at various temperatures. The results are compared with results obtained on a small-crystal (0.5 μm) Pt/H–mordenite, for which diffusion limitations can be excluded. Furthermore, an attempt is made to explain the results using a mathematical model for single-file diffusion and hydroisomerization on Pt/H–mordenite.

METHODS AND MATERIALS

Catalyst Preparation and Characterization

Large crystals of Na–mordenite were prepared according to a method described in Ref. (9). The obtained material was characterized using X-ray diffraction (XRD) and was identified as mordenite; no (crystalline) contaminations were detected in the XRD pattern.

Na–mordenite with a Si/Al of 10 and a crystal size of ~0.5 μm was obtained from Shell Research and Technology Centre in Amsterdam, The Netherlands. The size of the large mordenite crystals was determined using scanning electron microscopy (SEM). The sample was found to contain mainly crystals of ~50 μm but small amounts of small crystals (<1 μm) were also present.

The Na^+ ions were substituted for NH_4^+ ions by exchanging them in a solution of NH_4NO_3 and the obtained NH_4–mordenite was calcined to give H–mordenite. The H–mordenite samples were loaded with Pt by ion exchange in a solution of $Pt(NH_3)_4(NO_3)_2$, followed by careful calcination and reduction. The amount of Pt in the solution corresponded to a catalyst loading of 2 wt% on complete exchange, which for the given Si/Al is enough to ensure that the alkane/alkene equilibrium is established (10). Ultraviolet–visible (UV/VIS) measurements of the filtrate showed that the exchange was complete. The concentration of Brønsted acid sites was determined using temperature-programmed decomposition (TPD) of isopropylamine (11). Experimental details with regard to the catalyst preparation and characterization are reported in Ref. (12).

In Table 1 the characteristics of the two mordenite samples are reported. It is remarkable that the concentration of Brønsted sites of the 50-μm H–mordenite sample seems to be much lower than that of the small-crystal sample,

TABLE 1

Catalyst Characteristics

Property	0.5-μm sample	50-μm sample
Si/Al ratio	10	10
Crystal size (μm)	0.5	50
Pt concentration (wt%)	3	2
Concentration of Brønsted acid sites (mol/g)	5.7×10^{-4}	1.1×10^{-4}

although the Si/Al ratios are the same. A possible explanation is that the 50-μm sample contains a substantially larger amount of weak Brønsted acid sites, which are known to be inactive in isopropylamine decomposition (13), compared to the 0.5-μm sample. This is confirmed by results of ammonia TPD, which showed a considerably lower-onset temperature for the 50-μm sample (180° vs. 300°C).

Equipment

A continuous flow reactor was used, consisting of a quartz tube reactor (internal diameter, 4 mm) filled with catalyst pellets, which was placed inside an oven. The pellets were prepared by compressing the zeolite powder for 1 min at a pressure of 1.6 tons per cm^2, followed by crushing and sieving; the sieve fraction of 125–500 μm was used for the experiments. Gas-phase mixtures of *n*-hexane (Merck, >99%) and hydrogen were obtained using a Bronckhorst CEM (Controller/Evaporator/Mixer) unit, consisting of a liquid mass flow controller for *n*-hexane, a mass flow controller for hydrogen, and a heated mixing chamber. An additional mass flow controller was used for adding controlled amounts of nitrogen in order to vary alkane concentrations at constant hydrogen pressure and space velocity. The gas mixtures were flowed through the catalyst bed and the reaction products were analyzed on-line with a HP5890 series II gas chromatograph containing a Chrompack fused silica column with a Al_2O_3/KCl coating and a flame ionization detector.

Conditions

The measurements were carried out at atmospheric pressure and at temperatures between 493 and 573 K. A total flow of 150 Nml/min was used, consisting of 140 Nml/min hydrogen, 2.5–10 Nml/min *n*-hexane, and 0–7.5 Nml/min nitrogen. As the differential method of kinetic analysis was used, the amounts of catalyst were tuned so as to keep conversions below 10%. Thus, between 56 and 95 mg of 50-μm Pt/H–mordenite and between 17 and 68 mg of 0.5-μm Pt/H–mordenite were used.

Individual activity measurements were performed after a short time on stream (5 min) in order to minimize the influence of deactivation on the measured activity. After each activity measurement, the catalyst was regenerated at 450°C in flowing hydrogen for 2 h.

The *TOF*s that were used for data analysis were calculated from the total conversion toward all hexane isomers and propane, which is a secondary product since it can be formed by type C cracking of 2-methylpentane (14). However, propane can also be a product of the main side reactions that can occur (i.e., hydrogenolysis and dimerization cracking). Since it may be impossible to separate the different contributions to the propane production, this could introduce an error in the calculated *TOF*s.

MODELING

For single-file diffusion, in contrast to diffusion in pore systems with higher connectivities, the correlation between the displacement of individual molecules does not vanish at long observation times (15), leading to deviations from Einstein's diffusion equation, which is given by

$$\langle r^2(t)\rangle = 2Dt, \qquad [3]$$

where $\langle r^2(t)\rangle$ denotes the mean square displacement of a molecule, t the observation time, and D the effective diffusion coefficient. Fedders (16) derived an equation for $\langle r^2(t)\rangle$ under conditions of single-file diffusion in pores of infinite length, which is valid if it is assumed that (i) diffusion occurs as a sequence of jumps between adjacent sites and (ii) jump attempts are only succesful if the sites to which they are directed are vacant. His equation is

$$\langle r^2(t)\rangle = 2l\frac{1-\theta}{\theta}\sqrt{\frac{D_0 t}{\pi}}, \qquad [4]$$

where l is the distance between two adjacent sites, θ the fraction of occupied sites, and D_0 the diffusion coefficient of a single particle. Two important differences with "ordinary" diffusion, as described by Eq. [3], can be distinguished. In the first place, $\langle r^2(t)\rangle$ is proportional to $\sqrt{t}$ rather than to t. In the second place, the increase of the mobility in the limit of zero coverage is much larger than in the case of "ordinary" concentration-dependent diffusion, as occurs in microporous materials with a higher pore connectivity. Hahn *et al.* (17) and Nelson *et al.* (18) have pointed out that there is a second mode of molecular transport in one-dimensional pores caused by a shifting of the center of mass, which is superimposed on the single-file mode described by Eq. [4]. Because such a shift necessitates a shifting of all the particles in the same direction, the motion of the center of mass and the motion of the individual particles are identical. According to Nelson *et al.* (18), the center-of-mass motion is dominant for observation times much longer than a characteristic crossover time t_c,

$$t_c = \frac{(L-l)^2}{\pi D_0}, \qquad [5]$$

where L denotes the pore length. In contrast to the type of single-file diffusion described by Fedder's relation, for center-of-mass diffusion, $\langle r^2(t)\rangle$ is proportional to t, as for ordinary diffusion. For long files ($L/l \gg 1$), the effective diffusion coefficient that arises from the center-of-mass motion, D_{cm}, is given by (17–19)

$$D_{cm} = D_0\frac{(1-\theta)}{\theta N}, \qquad [6]$$

where N is the number of sites in the pore ($N = L/l$). Like the type of diffusion described by Eq. [4], this type

of diffusion is uniquely related to diffusion in a single file, so the term single-file diffusion is somewhat ambiguous. Therefore, we will refer to the type of single-file diffusion described by Eq. [4] as classic single-file diffusion and to the other type as center-of-mass single-file diffusion.

From other work, the intrinsic kinetics of the hydroisomerization of *n*-hexane on a number of platinum-loaded acidic zeolites, including H–mordenite, has been determined (12, 20). Here we derive an equation that describes *n*-hexane hydroisomerization on Pt/H–mordenite under conditions of single-file diffusion limitation and employ the values of the intrinsic kinetic parameters to predict the *TOF* as a function of *n*-hexane pressure and temperature.

First, it is necessary to decide which of the two single-file diffusion regimes is appropriate to describe mass transfer in the catalyst. The work described in Refs. (12, 20) has demonstrated that within the temperature range of our experiments, k_{isom} has a value of the order of 10^{-2} s^{-1}. On the other hand, a computed value of the self-diffusion coefficient for *n*-hexane in mordenite at low occupancy is $\sim 10^{-8}$ m^2/s (21), which can be used as a lower limit for the value of D_0. Filling in this value in Eq. [5] gives $t_c \sim 10^{-1}$ s ($L = 5\times 10^{-5}$ m). As this value is much smaller than $1/k_{isom}$, it can be concluded that the dominant mode of molecular transport is center-of-mass single-file diffusion.

The second step is to write down the steady-state mass balance for the reacting surface species (i.e., the alkoxy species formed by subsequent dehydrogenation and protonation of *n*-hexane molecules),

$$D_{cm}\frac{d^2\theta_n}{dx^2} - k_{isom}\theta_{nC6\,alkoxy} = 0, \qquad [7]$$

where θ_n is the surface occupancy of all *n* species (*n*-hexane, *n*-hexenes, *n*-hexyl alkoxides). To solve this equation, either θ_n or $\theta_{nC6\,alkoxy}$ has to be eliminated. Using Eqs. [A4] and [A5] (see Appendix), θ_n can be expressed in terms of $\theta_{nC6\,alkoxy}$:

$$\begin{aligned}\theta_n &= \theta_{nC6} + \theta_{nO6} + \theta_{nC6\,alkoxy}\\ &= \frac{p_{H_2}}{K_{dehydr}K_{prot}}\theta_{nC6\,alkoxy} + \frac{1}{K_{prot}}\theta_{nC6\,alkoxy} + \theta_{nC6\,alkoxy}. \qquad [8]\end{aligned}$$

Combining Eqs. [7] and [8] gives

$$D_{cm}\left(\frac{p_{H_2}}{K_{dehydr}K_{prot}} + \frac{1}{K_{prot}} + 1\right)\frac{d^2\theta_{nC6\,alkoxy}}{dx^2} - k_{isom}\theta_{nC6\,alkoxy} = 0. \qquad [9]$$

As was done in deriving Eq. [1], it is assumed that the reverse reaction can be neglected. Assuming the boundary conditions (0 and $(1/2)L$ are the coordinates, respectively, of the center of the catalyst and the gas–solid interface; the superscript *i* refers to the gas–solid interface)

$$\frac{d\theta_{nC6\,alkoxy}(0)}{dx} = 0, \qquad [10]$$

$$\theta_{nC6\,alkoxy}\left(\frac{1}{2}L\right) = \theta^i_{nC6\,alkoxy}, \qquad [11]$$

the solution of Eq. [9] is (8)

$$\theta_{nC6\,alkoxy}(x) = \theta^i_{nC6\,alkoxy}\frac{\cosh\phi\frac{x}{2L}}{\cosh\phi}. \qquad [12]$$

The parameter ϕ is comparable to the Thiele modulus for a surface reaction that is first order in θ (8) and is represented by

$$\phi = \frac{1}{2}L\sqrt{\frac{k_{isom}K_{dehydr}K_{prot}}{(p_{H_2} + K_{dehydr} + K_{dehydr}K_{prot})D_{cm}}}. \qquad [13]$$

The mean *TOF* can be calculated by multiplying k_{isom} by the mean concentration of reacting *n*-alkoxy molecules, $\bar{\theta}_{nC6\,alkoxy}$, which in turn is obtained by integrating Eq. [12] over the interval 0 to $(1/2)L$ and dividing by $(1/2)L$:

$$\overline{TOF} = k_{isom}\bar{\theta}_{nC6\,alkoxy} = k_{isom}\theta^i_{nC6\,alkoxy}\frac{\tanh\phi}{\phi}. \qquad [14]$$

The factor $(\tanh\phi)/\phi$ is known as the effectiveness factor. If it is assumed that adsorption and desorption at the gas–solid phase is infinitely fast and that the gas-phase concentration of reaction products can be neglected, then $\theta^i_{nC6\,alkoxy}$ is equal to the equilibrium occupancy of *n*-alkoxides if there is no catalytic activity (see Appendix):

$$\theta^i_{nC6\,alkoxy} = \frac{K_{ads}K_{dehydr}K_{prot}\frac{p_{nC6}}{p_{H_2}}}{1 + K_{ads}p_{nC6} + K_{ads}K_{dehydr}\frac{p_{nC6}}{p_{H_2}} + K_{ads}K_{dehydr}K_{prot}\frac{p_{nC6}}{p_{H_2}}}. \qquad [15]$$

The third step is to derive an expression for D_{cm} that includes the influence of the alkoxy intermediates. Since the protonation energy of hexene was found to be equal to −44 kJ/mol (12), this means that the activation energy of deprotonation is at least 44 kJ/mol. Hence, it is reasonable to assume that the alkoxy species are effectively immobile. For observation times much longer than the time constants of (de)protonation (i.e., the reciprocal rate coefficients of (de)protonation), it may be expected that the single-particle diffusion coefficient is reduced by a factor equal to the probability *W* that the molecule is mobile,

$$D'_{0,k} = W_k D_{0,k}, \qquad [16]$$

where $D'_{0,k}$ denotes the corrected single-particle diffusion coefficient of an isolated molecule with skeletal arrangement *k*, and W_k can be assumed to be equal to the fraction of mobile species (i.e., the fraction of adsorbed molecules

consisting of hexanes and hexenes),

$$W_k = \frac{\theta_{k,C6} + \theta_{k,O6}}{\theta_{k,C6} + \theta_{k,O6} + \theta_{k,C6\,alkoxy}}. \quad [17]$$

The center-of-mass diffusion coefficient during hydroisomerization can then be represented by the following equation:

$$D_{cm} = D_0^{eff} W^{eff} \frac{(1-\theta)}{\theta N}. \quad [18]$$

The effective parameters D_0^{eff} and W^{eff} are functions of $D_{0,1}, \ldots, D_{0,n}, W_{0,1}, \ldots, W_{0,n}, \theta_1, \ldots, \theta_n$ with the index $1, \ldots, n$ denoting the various isomers. If it is assumed that the values of K_{ads}, K_{dehydr}, and K_{prot} are the same for all hexane isomers, then θ and W^{eff} are given by (see Appendix)

$$\theta = \theta_{C6} + \theta_{O6} + \theta_{C_6\,alkoxy} = \frac{K_{ads}p_{nC6} + K_{ads}K_{dehydr}\frac{p_{nC6}}{p_{H_2}} + K_{ads}K_{dehydr}K_{prot}\frac{p_{nC6}}{p_{H_2}}}{1 + K_{ads}p_{nC6} + K_{ads}K_{dehydr}\frac{p_{nC6}}{p_{H_2}} + K_{ads}K_{dehydr}K_{prot}\frac{p_{nC6}}{p_{H_2}}}, \quad [19]$$

$$W^{eff} = \frac{\theta_{C6} + \theta_{O6}}{\theta} = \frac{p_{H_2} + K_{dehydr}}{p_{H_2} + K_{dehydr} + K_{dehydr}K_{prot}}. \quad [20]$$

Finally, combining Eqs. [13]–[15] and [18]–[20] and substituting N with L/l gives the following equation for the mean TOF:

$$\overline{TOF} = \frac{2\sqrt{k_{isom}D_0^{eff}lK_{ads}K_{dehydr}K_{prot}p_{nC6}(p_{H_2} + K_{dehydr})}}{\left(1 + K_{ads}p_{nC6} + K_{ads}K_{dehydr}\frac{p_{nC6}}{p_{H_2}} + K_{ads}K_{dehydr}K_{prot}\frac{p_{nC6}}{p_{H_2}}\right)L^{3/2}} \times \frac{\tanh\sqrt{\frac{k_{isom}L^3K_{ads}K_{dehydr}K_{prot}}{4D_0^{eff}lp_{H_2}}\left(1 + \frac{K_{dehydr}K_{prot}}{p_{H_2}+K_{dehydr}}\right)p_{nC6}}}{\sqrt{p_{H_2}(p_{H_2} + K_{dehydr} + K_{dehydr}K_{prot})}}. \quad [21]$$

Now we have an expression for the mean TOF in terms of parameters whose values either are imposed (p_{nC6}, p_{H_2}) or can be determined from independent experiments (N, D_0^{eff}, k_{isom}, K_{ads}, K_{dehydr}, K_{prot}). N can be calculated by dividing L by l. l, in turn, can be estimated by dividing the maximum amount of *n*-hexane that can be adsorbed per unit cell by the total pore length per unit cell, assuming that one site can accommodate precisely one molecule. Eder measured the maximum loading c_{max} of *n*-hexane in H–mordenite with a Si/Al ratio of 10 and found it to be equal to 0.58 mol/kg (22). Using the generalized formula for the unit cell of H–mordenite, $H_n[Al_nSi_{48-n}O_{96}]\cdot 24H_2O$, the maximum *n*-hexane concentration per unit cell $c_{max,u.c.}$ can be calculated by multiplying c_{max} by the mass of a mole unit cell (3.316 kg). Since the length of the unit cell in the direction of the pores is 7.5 Å and the density of pores is 2 per unit cell (23), the mean length (in Å) of an *n*-hexane molecule and hence l is equal to $15/c_{max,u.c}$. K_{ads} was calculated using literature values for the adsorption enthalpy, with the maximum *n*-hexane loading and the adsorption constant measured at 323 K (22). K_{dehydr} was calculated from the standard enthalpy and entropy of formation of *n*-hexane and "hexene" (for the latter, the average entropy and enthalpy of formation of all hexene isomers was taken) using the equation

$$K_{dehydr}(T) = \exp\left(\frac{\Delta S^{\theta}_{dehydr}}{R} - \frac{\Delta H^{\theta}_{dehydr}}{RT}\right)p^{\theta}, \quad [22]$$

where $\Delta S^{\theta}_{dehydr}$ and $\Delta H^{\theta}_{dehydr}$ are, respectively, the standard entropy and enthalpy of dehydrogenation and p^{θ} is the standard pressure ($p^{\theta} = 101325$ Pa). Although $\Delta S^{\theta}_{dehydr}$ and $\Delta H^{\theta}_{dehydr}$ refer to a gas-phase reaction, it was assumed that their values were the same as for dehydrogenation in the adsorbed phase. The values of $\Delta S^{\theta}_{dehydr}$ and $\Delta H^{\theta}_{dehydr}$ were extracted from Ref. (24). As mentioned earlier, k_{isom} and K_{prot} were calculated using data measured by De Gauw *et al.* (12, 20). With regard to D_0^{eff}, no reliable value could be obtained, mainly owing to a lack of literature data. Although Schuring *et al.* determined the self-diffusion coefficients of a number of alkanes in mordenite (21), these data were obtained at finite occupancies and hence are not good estimates for D_0^{eff}. Therefore, D_0^{eff} was chosen so as to obtain the best fit between the experimental data and Eq. [21]. A single value for D_0^{eff} was used for the whole alkane pressure and temperature range. This implies that the activation energy of D_0^{eff} was assumed to be negligibly small and that possible effects of changes in the concentration fractions on D_0^{eff} as a result of varying pressure and temperature are neglected. The first assumption is supported by results of molecular dynamics simulations, according to which the activation energy of *n*-hexane diffusion in mordenite is 2.3 kJ/mol (21).

The values of the temperature-independent model parameters (except for D_0^{eff}) and the quantities that were used to calculate the temperature-dependent model parameters are listed in Table 2. On the basis of the parameter values represented in Table 2, the order of the intrinsic reaction

TABLE 2

Parameters Used for Model Calculations

Parameter	Value	Parameter	Value
L (m)	5×10^{-5}	$\Delta S^{\theta}_{dehydr}$ (J/mol/K)	126
l (m)	7.9×10^{-10}	$\Delta H^{\theta}_{dehydr}$ (kJ/mol)	118
ν_{isom} (s^{-1})	2.3×10^{10}	K^0_{prot}	28
$E_{act,isom}$ (kJ/mol)	117	ΔH_{prot} (kJ/mol)	−44
K^0_{ads} (Pa^{-1})	1.4×10^{-11}	p_{nC6} (kPa)	1.7–6.7
ΔH_{ads} (kJ/mol)	−69	p_{H_2} (kPa)	95

Note. ν_{isom} and $E_{act,isom}$ are, respectively, the preexponential factor and activation energy of the elementary isomerization step; K^0_{ads} and K^0_{prot} are, respectively, the preexponential factors of K_{ads} and K_{prot}.

with respect to *n*-hexane was predicted to be approximately 0.3, irrespective of temperature.

RESULTS AND DISCUSSION

Experimental Results

As was stated in Methods and Materials, the occurrence of side reactions may introduce an error in the calculated *TOF*s. A study of the product distributions may be helpful in estimating this error. In the case of the 0.5-μm sample, the mole fraction of products consisting of isomers was more than 96 mol%, so the effect of side reactions could be neglected. However, in the case of the 50-μm sample, the fraction of isomers comprised between 60 and 90 mol% of the products, with the rest consisting of cracking products; no significant amounts of products longer than C6 were detected. As almost no methane and ethane were detected, it was concluded that the hydrogenolysis activity was negligible. The cracked products contained between 40 and 70% C4 and C5 isomers, indicating that the sample had a considerable dimerization cracking activity. The highest selectivity toward propane that was observed was 26 mol%, which means that at most 13% of the reacting *n*-hexane molecules was converted into propane. Since it was not known how large the fraction of propane was that was formed by monomolecular cracking, the resulting error in the *TOF* was estimated to be a maximum of 13%. However, this does not affect the trend in the reciprocal rate equation plots that is predicted in the case of single-file diffusion limitations. Since dimerization cracking is a bimolecular reaction, the corresponding reaction rate will increase faster with increasing *n*-hexane pressure than will the rate of isomerization. Therefore, the fraction of propane that results from dimerization cracking increases as the *n*-hexane pressure increases, so the lowering of the *TOF* with respect to the intrinsic *TOF* is underestimated more at high pressure than at low pressure. Because single-file diffusion limitation leads to an increase in the difference between the observed and the intrinsic reaction rate with increasing pressure, correction for the influence of dimerization cracking would only enhance this trend.

In Fig. 1, reciprocal rate equation plots for *n*-hexane hydroisomerization on the 0.5- and 50-μm samples at 220°C are shown. At the lowest applied pressure (highest $1/p_{nC6}$), the ratio between the *TOF* of the 0.5-μm sample and that of the 50-μm sample is 0.96, which increases to 1.4 at the highest applied pressure. This is just what is expected if diffusion limitation occurs and the effective diffusion coefficient decreases with increasing surface concentration. Moreover, the plot of the 50-μm sample displays the deviation from linearity which was predicted in case of concentration-dependent diffusion limitation.

Figures 2 and 3 represent reciprocal rate equation plots obtained with the 50-μm sample at various temperatures.

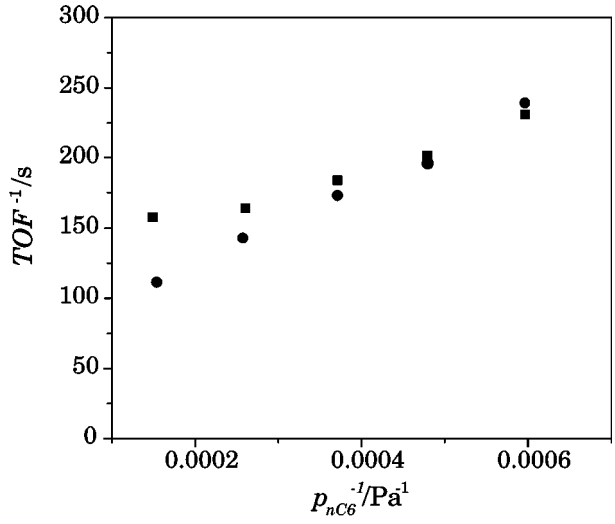

FIG. 1. Comparison between reciprocal rate equation plots obtained with the 0.5-μm and 50-μm samples at $T = 220$°C (■, 50-μm sample; ●, 0.5-μm sample).

The most striking feature of the plots is the appearance of a minimum; in other words, there is a maximum in the *TOF* as a function of pressure. This can be explained as follows: at low surface concentrations, the decrease in mobility with increasing concentration is so small, that no inhibiting effect on the *TOF* is observed. However, at a certain concentration, the pores become so crowded that the increase in the *TOF* that would occur in the absence of diffusion limitation as a result of the higher concentration is overcompensated for by the decrease in mobility, leading to an overall lowering of the *TOF*. This is illustrated by Fig. 4, in which the intrinsic turnover frequency TOF_{intr}, the effectiveness factor η under conditions where Eq. [6] is valid, and the resulting overall turnover frequency TOF_{cm} ($= TOF_{intr}\,\eta$)

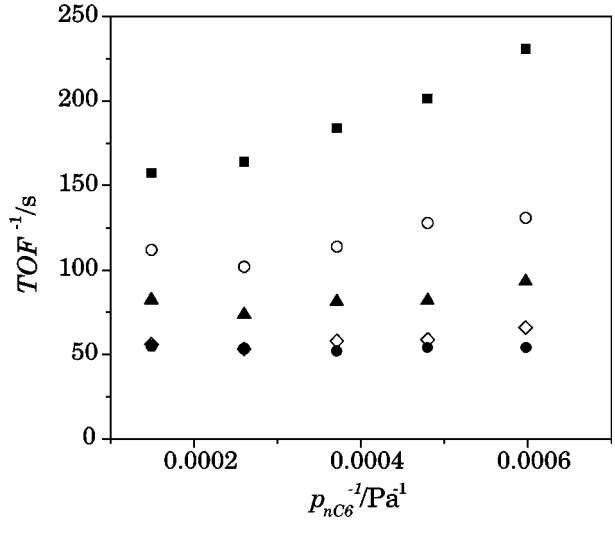

FIG. 2. Experimental reciprocal rate equation plots obtained with the 50-μm sample (■, 220°C; ○, 230°C; ▲, 240°C; ◇, 250°C; ●, 260°C).

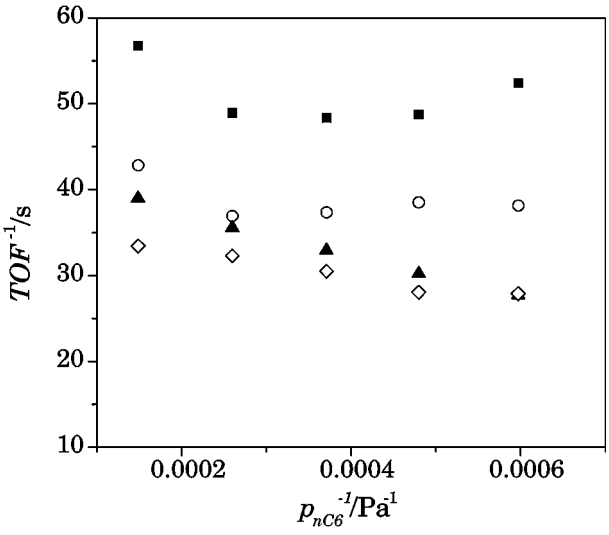

FIG. 3. Experimental reciprocal rate equation plots obtained with the 50-μm sample (■, 270°C; ○, 280°C; ▲, 290°C; ◇, 300°C).

for a reaction that is first order in θ is plotted as a function of p (assuming that adsorption can be described by a Langmuir isotherm).

Figures 2 and 3 also show that the minimum shifts toward higher $1/p$ with increasing temperature. To explain this we must closely examine the data presented in Table 2. On the basis of these data, some remarkable features of the system can be discerned. In the first place, within the experimental temperature range, alkoxy species are the dominant species (for instance, at 250°C, $\theta_{nC6\,alkoxy} = 0.82$), and as the enthalpy difference between gas-phase *n*-hexane and alkoxy species ($\Delta H_{ads} + \Delta H_{dehydr} + \Delta H_{prot}$) is only 5 kJ/mol (see Table 2), θ is almost invariant with temperature. This has important consequences for the temperature dependence of the effectiveness factor. This dependence is quite different for concentration-dependent diffusion compared to concentration-independent diffusion; in the latter case, η decreases with increasing temperature because the activation energy of the reaction rate coefficient is generally higher than the activation energy of diffusion, causing the intrinsic activity to increase faster with temperature than the rate of diffusion. However, in the case of concentration-dependent diffusion, the effective diffusion coefficient is expected to increase much faster with temperature, owing to the decreasing θ (see Eq. [6]). The variation of the extent of diffusion limitation with temperature is determined by the combined action of opposing effects, and so the direction of the change depends on the variation of their relative importance. In the case of hydroisomerization, however, the surface concentration is only a weak function of temperature, so the shifting of the position of the minimum is determined largely by the effect of the changing value of k_{isom}. As a result, the minimum shifts continuously toward higher values of $1/p$ as the temperature increases.

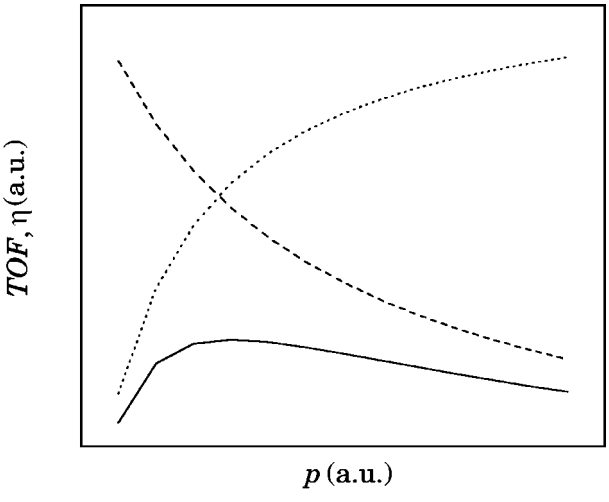

FIG. 4. Effect of center-of-mass single-file diffusion on the *TOF* of a surface reaction that is first order in θ. (···) TOF_{intr}, (- - -) η, and (——) TOF_{cm}.

A further notable feature of Figs. 2 and 3 is the seemingly small variation of the *TOF* with temperature, especially at higher temperatures, as is shown by the fact that the curves lie very close to each other. Indeed, at $p_{nC6} = 2658$ Pa, the apparent activation energy was found to vary between 91 kJ/mol (in the temperature interval 220–260°C) and 21 kJ/mol (in the temperature interval 260–300°C); according to results of De Gauw *et al.*, the apparent activation energy for *n*-hexane hydroisomerization on Pt/H–mordenite measured under conditions where the reaction was rate limiting was 126 kJ/mol (12). At first sight this seems a puzzling result since single-file diffusion limitation has been proposed to cause an enhancement of the apparent activation energy (25). If the effective diffusion coefficient were independent of concentration, the apparent activation energy should be equal to half the intrinsic activation energy (8). Therefore, the results suggest that the effective diffusion coefficient decreases with increasing temperature. This is understood by calling to mind Eq. [20] and recognizing that since $K_{dehydr} \ll p_{H_2}$ (see Table 2), this equation can be approximated by

$$W^{eff} \approx \frac{p_{H_2}}{p_{H_2} + K_{dehydr} K_{prot}}. \qquad [23]$$

As $\Delta H_{dehydr} + \Delta H_{prot} > 0$ the denominator increases and consequently W^{eff} decreases with increasing temperature. Since it was already observed that the total concentration of surface species is almost independent of temperature, the result is that the effective diffusion coefficient decreases as the temperature increases.

Model Calculations

As was pointed out earlier, the lack of a reliable value for D_0^{eff} made it necessary to make an estimate. We chose

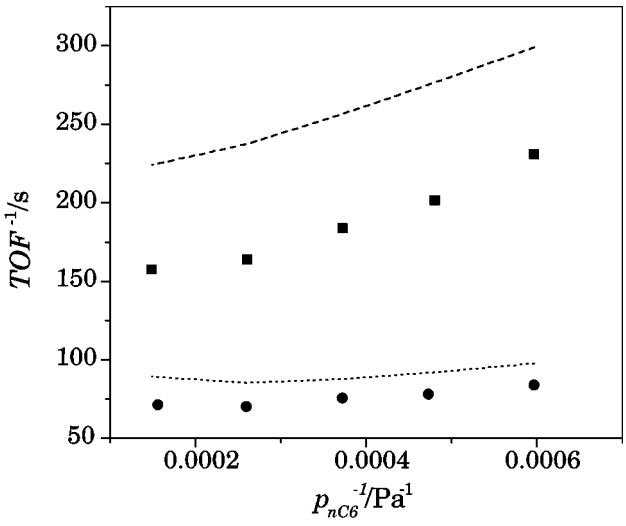

FIG. 5. Experimental (discrete points) and modeled (dotted lines) reciprocal rate equation plots for *n*-hexane hydroisomerization on the 50-μm sample; model *including* effect of immobile species. (■, - - -) 220°C; (●, · · ·) 240°C.

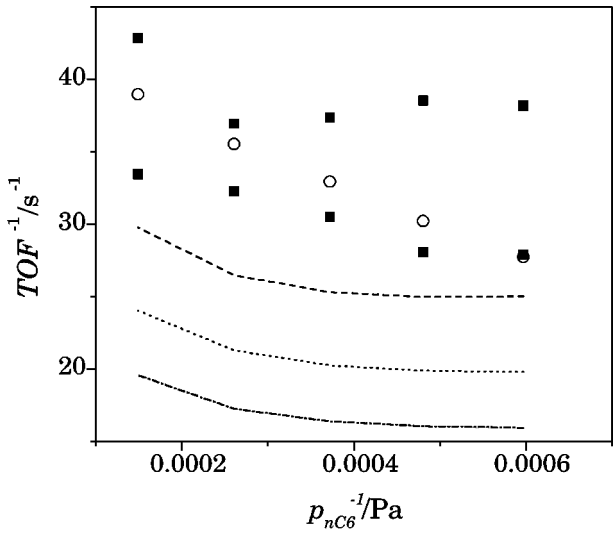

FIG. 7. Experimental (discrete points) and simulated (dotted lines) reciprocal rate equation plots for *n*-hexane hydroisomerization on the 50-μm sample; model *excluding* effect of immobile species. (■, - - -) 260°C; (●, · · ·) 280°C; (▲, -·-·-·) 300°C.

to use D_0^{eff} as a fitting parameter, that is to adjust its value in such a way as to obtain the best agreement between simulation and experiment. By applying Eq. [21], the experimental data could be fitted quite well with a single D_0^{eff} for the whole temperature range (see Figs. 5 and 6). The best fit (correlation coefficient = 0.9933) was obtained for $D_0^{eff} = 8.1 \times 10^{-6}$ m^2/s. The order of magnitude of D_0^{eff} agrees well with that of experimentally determined single-particle diffusion coefficients of methane, ethane, and tetrafluormethane in various molecular sieves (26–29). It is important to emphasize that in order to obtain a good agreement between experiment and model, it was essential to include a correction factor for the influence of immobile species on the rate of diffusion in the model; without this correction, the agreement between model and experiment after optimization of the fit was much worse, especially at high temperatures (see Fig. 7).

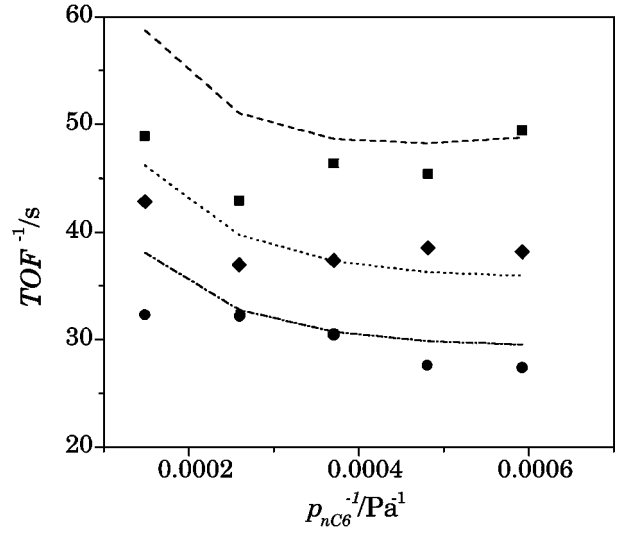

FIG. 6. Experimental (discrete points) and modeled (dotted lines) reciprocal rate equation plots for *n*-hexane hydroisomerization on the 50-μm sample; model *including* effect of immobile species. (■, - - -) 260°C; (●, · · ·) 280°C; (▲, -·-·-·) 300°C.

The good agreement between modeled and measured data provides evidence for two important issues in (acid) catalysis, namely the occurrence of anomalous effects on the kinetics of catalyzed reactions due to single-file diffusion and the existence of immobile alkoxy species. Furthermore, it has been demonstrated that the effects of these phenomena can be modeled by using the concept of center-of-mass single-file diffusion, as represented by Eq. [6] and assuming that the diffusion coefficient is proportional to the fraction of mobile adsorbed species. The modeling of the effects of single-file diffusion and/or immobile species on mass transfer as presented here may be extended to other catalyzed reactions as well and may be useful for optimizing process conditions and catalyst dimensions. As an example, a criterion for diffusion limitation for the catalytic system of the present study is derived. Generally, diffusion limitations can be neglected if $\phi \ll 1$. In Eq. [21], ϕ can be identified as

$$\phi = \sqrt{\frac{k_{isom} L^3 K_{ads} K_{dehydr} K_{prot}}{4 D_0^{eff} l p_{H_2}} \left(1 + \frac{K_{dehydr} K_{prot}}{p_{H_2} + K_{dehydr}}\right) p_{nC6}}. \quad [24]$$

This equation can be used to predict under which conditions diffusion limitation will occur. Here we consider

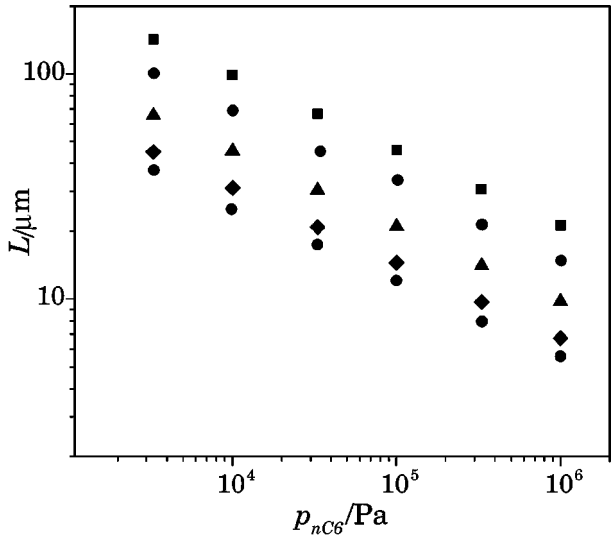

FIG. 8. Crystal size as a function of *n*-hexane pressure at which $\eta = 0.9$ for various temperatures (■, 230°C; ○, 250°C; ▲, 270°C; ◇, 290°C; ●, 300°C).

diffusion limitation to be significant if $\eta < 0.9$, which corresponds to $\phi = 0.58$. In Fig. 8, the crystal size at which $\phi = 0.58$ is plotted as a function of p_{nC6} at various temperatures. The required values for K^0_{ads}, K^0_{dehydr}, K^0_{prot}, ν_{isom}, ΔH_{ads}, ΔH_{dehydr}, ΔH_{prot}, and $E_{act,isom}$ were taken from Table 2, while for D_0^{eff} the value obtained by fitting the experimental results to Eq. [21] was used; p_{H_2} was taken to be equal to 20 bar, which is within the operating range of industrial hydroisomerization. Because the plots in Fig. 8 have the form $L = constant \cdot p_{nC6}^{-1/3}$ (see Eq. [24]), logarithmic plotting gives parallel lines with a slope equal to $-1/3$. Figure 8 may be interpreted as follows: if for a given temperature, crystal radius, and pressure (L, p_{nC6}) lies above the line corresponding to $\phi = 0.58$, diffusion limitation is significant. For example, the total isomerization process (TIP), which is the most common industrial hydroisomerization process in which Pt/H–mordenite is the catalyst, is operated at a temperature of 250°C, a p_{H_2} of 10–30 bar, and a $p_{H_2}/(p_{nC5} + p_{nC6})$ of 10 (the alkane feedstock consists of a mixture of *n*-pentane and *n*-hexane). According to Fig. 8, for $p_{H_2} = 20$ bar and $p_{nC6} = 2$ bar (*n*-pentane is ignored), diffusion limitation will become significant for crystal sizes larger than 16 μm. As this radius is much higher than the typical radii of commercial catalysts (for instance, the radius of the small crystal mordenite used in this study, which is a commercial sample, is ~0.5 μm), it can be concluded that in the TIP micropore, diffusion is not rate limiting.

CONCLUSIONS

The intrinsic kinetics of *n*-hexane hydroisomerization can be described by a rate equation according to which the reciprocal reaction rate is a linear function of the reciprocal *n*-hexane pressure. However, if diffusion is rate limiting and the diffusion coefficient decreases with increasing surface concentration θ, deviations from this linearity may be observed at low values of the reciprocal pressure (high θ). The explanation for such a deviation is that the linear decrease in the intrinsic reaction rate with decreasing $1/\theta$ is reduced by a factor that becomes larger as $1/\theta$ decreases. Concentration-dependent diffusion is most likely to occur in the case of diffusion in one-dimensional pores which are too narrow for adsorbed molecules to be able to pass each other, causing the motion of individual molecules to become strongly correlated (single-file diffusion). Indeed, the expected deviations from the intrinsic rate equation were observed for *n*-hexane hydroisomerization on 50-μm crystals of Pt/H–mordenite, which has one-dimensional pores that are too narrow to allow counterdiffusion of *n*-hexane molecules.

For a reaction that occurs in a single-file pore and that is first order in θ, a rise of temperature has two opposite effects: on the one hand, the reaction rate coefficient increases, which causes diffusion to become rate limiting at lower θ; on the other hand, the adsorption constant and therefore θ at a given pressure decreases, leading to an increase in the effective diffusion coefficient. However, for the reaction studied here, there are important deviations from this predicted general pattern. These deviations probably originate from the abundance of immobile alkoxy species, which are produced as reaction intermediates, in the zeolite pores. Because the alkoxy species are the dominant surface species and the enthalpy difference between gas-phase alkane and alkoxy species is only 5 kJ/mol, the change of θ is negligible within a wide temperature range. Since the enhancing effect of a decrease of θ on the effective diffusion coefficient is now absent, the single-file effects become stronger with increasing temperature owing to the increasing isomerization rate coefficient. Moreover, at the same time, the effective diffusion coefficient is expected to decrease, because the alkoxy species are immobile and the equilibrium between alkoxy species and adsorbed alkanes shifts toward the alkoxy side. The effect of single-file diffusion and the presence of immobile surface species on the kinetics of *n*-hexane hydroisomerization was modeled using a mathematical model based on the relation between the diffusion coefficient and the fraction of occupied sites under single-file conditions, as proposed by Hahn *et al.* and Nelson *et al.* Except for the effective single-particle diffusion coefficient D_0^{eff}, for which no reliable literature value was found, the values of the input parameters were taken from independent studies, and to model the effect of immobile species, it was assumed that D_0^{eff} was proportional to the relative concentration of alkanes in the pores. A good agreement over the whole temperature range was obtained by assuming $D_0^{eff} = 8.1 \times 10^{-6}$ m^2/s. The order of

magnitude of D_0^{eff} agrees well with that of experimentally determined single-particle diffusion coefficients of methane and tetrafluormethane in various molecular sieves.

APPENDIX: DERIVATION OF EQ. [1]

The reaction scheme is as follows.

1. Adsorption:

$$n\text{-}C_6H_{14}(g) + H\text{–}O\text{–}Z \rightleftarrows n\text{-}C_6H_{14}\text{–}H\text{–}O\text{–}Z.$$

2. Dehydrogenation:

$$\begin{aligned} n\text{-}C_6H_{14}\text{–}H\text{–}O\text{–}Z + Pt &\rightleftarrows n\text{-}C_6H_{14}\text{–}Pt + H\text{–}O\text{–}Z \\ n\text{-}C_6H_{14}\text{–}Pt + 3Pt &\rightleftarrows n\text{-}C_6H_{12}\text{–}Pt_2 + 2PtH \\ n\text{-}C_6H_{12}\text{–}Pt_2 + H\text{–}O\text{–}Z + 2PtH &\rightleftarrows n\text{-}C_6H_{12}\text{–}H\text{–}O\text{–}Z \\ &\quad + 4Pt + H_2 \\ \hline n\text{-}C_6H_{14}\text{–}H\text{–}O\text{–}Z &\rightleftarrows n\text{-}C_6H_{12}\text{–}H\text{–}O\text{–}Z + H_2. \end{aligned}$$

3. Protonation:

$$n\text{-}C_6H_{12}\text{–}H\text{–}O\text{–}Z \rightleftarrows n\text{-}C_6H_{13}\text{–}O\text{–}Z.$$

4. Isomerization:

$$n\text{-}C_6H_{13}\text{–}O\text{–}Z \rightarrow i\text{-}C_6H_{13}\text{–}O\text{–}Z.$$

Since the isomerization step is rate determining, the other steps are quasi equilibrated and are given by

$$\begin{aligned} r_{ads} = r_{des} &\Rightarrow k_{ads} p_{nC6}(1 - \theta_{nC6} - \theta_{nO6} - \theta_{nC6\,alkoxy}) \\ &= k_{des}\theta_{nC6}, \end{aligned} \quad [A1]$$

$$\frac{\theta_{nO6}}{\theta_{nC6}} = \frac{K_{dehydr}}{p_{H_2}}, \quad [A2]$$

$$\frac{\theta_{nC6\,alkoxy}}{\theta_{nO6}} = K_{prot}, \quad [A3]$$

where θ_{nO6} is the surface occupancy of *n*-hexenes. Rewriting and combining Eqs. [A2] and [A3] gives θ_{nC6} and θ_{nO6} in terms of $\theta_{nC6\,alkoxy}$:

$$\theta_{nO6} = \frac{1}{K_{prot}}\theta_{nC6\,alkoxy}, \quad [A4]$$

$$\theta_{nC6} = \frac{p_{H_2}}{K_{dehydr}}\theta_{nO6} = \frac{p_{H_2}}{K_{prot}K_{dehydr}}\theta_{nC6\,alkoxy}. \quad [A5]$$

Substituting θ_{nC6} and θ_{nO6} in Eq. [A1] with the right-hand sides of Eqs. [A4] and [A5] gives

$$k_{ads} p_{nC6}\left(1 - \frac{p_{H_2}}{K_{prot}K_{dehydr}}\theta_{nC6\,alkoxy} - \frac{1}{K_{prot}}\theta_{nC6\,alkoxy} - \theta_{nC6\,alkoxy}\right) = k_{des}\frac{p_{H_2}}{K_{prot}K_{dehydr}}\theta_{nC6\,alkoxy}. \quad [A6]$$

Rewriting Eq. [A6] gives the following expression for $\theta_{nC6\,alkoxy}$ (using the equality $k_{ads}/k_{des} = K_{ads}$):

$$\theta_{nC6\,alkoxy} = \frac{K_{ads}K_{dehydr}K_{prot}\frac{p_{nC6}}{p_{H_2}}}{\left(1 + K_{ads}p_{nC6} + K_{ads}K_{dehydr}\frac{p_{nC6}}{p_{H_2}} + K_{ads}K_{dehydr}K_{prot}\frac{p_{nC6}}{p_{H_2}}\right)}. \quad [A7]$$

According to the reaction scheme, the *TOF* is given by

$$TOF = k_{isom}\theta_{nC6\,alkoxy}. \quad [A8]$$

Finally, combining Eqs. [A7] and [A8] gives

$$TOF = \frac{k_{isom}K_{ads}K_{dehydr}K_{prot}\frac{p_{nC6}}{p_{H_2}}}{1 + K_{ads}p_{nC6} + K_{ads}K_{dehydr}\frac{p_{nC6}}{p_{H_2}} + K_{ads}K_{dehydr}K_{prot}\frac{p_{nC6}}{p_{H_2}}}. \quad [A9]$$

REFERENCES

1. Breck, D. W., "Zeolite Molecular Sieves: Structure, Chemistry and Use." Wiley-Interscience, New York, 1974.
2. Martino, G., Courty, P., and Marcilly, C., *in* "Handbook of Heterogeneous Catalysis" (G. Ertl, H. Knözinger, and J. Weitkamp, Eds.), p. 1806. VCH Verlagsgesellschaft, Weinheim, 1997.
3. Kazansky, V. B., *in* "Acidity and Basicity of Solids, Theory, Assessment and Utility" (J. Fraissard and L. Petrakis, Eds.), p. 335. Kluwer Academic, Dordrecht, 1994.
4. Van Santen, R. A., and Kramer, G. J., *Chem. Rev.* **95**, 637 (1995).
5. Weisz, P. B., *in* "Advances in Catalysis and Related Subjects" (D. D. Eley, P. W. Selwood, and P. B. Weisz, Eds.), Vol. 13, p. 137. Academic Press, New York, 1962.
6. Ribeiro, F., Marcilly, C., and Guisnet, M., *J. Catal.* **78**, 267 (1982).
7. Froment, G. F., *Catal. Today* **1**, 455 (1987).
8. Froment, G. F., and Bischoff, K. B., "Chemical Reactor Analysis and Design." Wiley, New York, 1990.
9. Warzywoda, J., Dixon, A. G., Thompson, R. W., Sacco, A., and Suib, S. L., *Zeolites* **16**, 125 (1996).
10. Gianetto, G. E., Perot, G. R., and Guisnet, M. R., *Ind. Eng. Chem. Prod. Res. Dev.* **25**, 481 (1986).
11. Juskelis, M. V., Slanga, J. P., Roberie, T. G., and Peters, A. W., *J. Catal.* **138**, 391 (1992).
12. De Gauw, F. J. M. M., Van Grondelle, J., and Van Santen, R. A., submitted for publication.
13. Biaglow, A. I., Parillo, D. J., and Gorte, R. J., *J. Catal.* **144**, 193 (1993).
14. Martens, J. A., Jacobs, P. A., and Weitkamp, J., *Appl. Catal.* **20**, 239 (1986).
15. Havlin, S., and Ben-Avraham, D., *Adv. Phys.* **36**, 695 (1987).
16. Fedders, P. A., *Phys. Rev. B* **17**, 40 (1978).
17. Hahn, K., and Kärger, J., *J. Phys. Chem. B* **102**, 5766 (1998).
18. Nelson, P. H., and Auerbach, S. M., *J. Chem. Phys.* **110**, 9235 (1999).
19. Rödenbeck, Ch., and Kärger, J., *J. Chem. Phys.* **110**, 3970 (1999).
20. Van Santen, R. A., and De Gauw, F. J. M. M., *Stud. Surf. Sci. Catal.* **130**, 127 (2000).

21. Schuring, D., Jansen, A. P. J., and van Santen, R. A., *J. Phys. Chem. B* **104**, 941 (2000).
22. Eder, F., Ph.D. thesis. University of Twente, Enschede, The Netherlands, 1996.
23. Meier, W. M., Olson, D. H., and Baerlocher, Ch., "Atlas of Zeolite Structure Types," 4th ed. Elsevier, Amsterdam/New York, 1996.
24. Stull, D. R., Westrum, E. F., and Sinke, G. C., "The Chemical Thermodynamics of Organic Compounds." Krieger, Melbourne, FL, 1987.
25. Rödenbeck, Ch., Kärger, J., and Hahn, K., *J. Catal.* **176**, 513 (1998).
26. Ylihautala, M., Jokisaari, J., Fischer, E., and Kimmich, R., *Phys. Rev. E* **57**, 6844 (1998).
27. Kukla, V., Kornatowski, J., Demuth, D., Girnus, I., Pfeifer, H., Rees, L. V. C., Schunk, S., Unger, K. K., and Kärger, J., *Science* **272**, 702 (1996).
28. Hahn, K., Kärger, J., and Kukla, V., *Phys. Rev. Lett.* **76**, 2762 (1996).
29. Gupta, V., Nirvarthi, S. S., McCormick, A. V., and Davis, H. T., *Chem. Phys. Lett.* **247**, 596 (1995).